Available online at www.sciencedirect.com
SCIENCE DIRECT
Physica B 376–377 (2006) 790–794
PHYSICA B
www.elsevier.com/locate/physb

Transition metals in $ZnGeP_2$ and other II–IV–V_2 compounds

W. Gehlhoff[a,*], D. Azamat[a,1], A. Hoffmann[a], N. Dietz[b], O.V. Voevodina[c]

[a]*Institute for Solid State Physics, Technical University Berlin, D-10623 Berlin, Germany*
[b]*Department of Physics and Astronomy, Georgia State University, Atlanta, GA 3030, USA*
[c]*Siberian-Physico-Technical Institute, 634050 Tomsk, Russia*

Abstract

Semiconductors that exhibit room-temperature ferromagnetism are central to the development of semiconductor spintronics. Transition metal (TM)-doped $A^{II}B^{IV}C_2^V$ are a promising class of such system. These ternary compound semiconductors have two metal sites A and B that can be substituted by the TMs. A site preference for TM incorporation is crucial for a possible explanation of ferromagnetism since dependent on the TM valent state holes or electrons can be released. For low Fe- and Cr-doped $ZnGeP_2$, our EPR investigations revealed in addition to the well-known native defects the presence of substitutional Fe^{2+} ($3d^6$, $S=2$) on Zn site, Fe^{3+} ($3d^5$, $S=\frac{5}{2}$) and Cr^{4+} ($3d^2$, $S=1$) on Ge site. A photo-induced recharging of Fe^{2+} to Fe^{+} is observed. The Cr^{4+} center exhibits a well-resolved phosphorus ligand hyperfine splitting. For Fe^{2+} and Fe^{3+}, the magnetic site inequivalence of each of the both Zn and Ge sites, respectively, has been detected. Moreover, anti-ferromagnetically coupled Mn^{2+}–Mn_{Zn}^{2+} pairs have been observed in Mn-doped $ZnGeP_2$.

PACS: 76.30.Fc; 75.50.Pp; 71.70.Gm; 70.50.+g

Keywords: EPR; $ZnGeP_2$; Mn; Fe; Cr; Valence state; Site inequivalence

1. Introduction

The exceptional properties of zinc germanium diphosphide ($ZnGeP_2$) and the recent improvements in the growth of high-quality bulk crystals by the horizontal gradient freeze (HGF) technique make this compound semiconductor to one of the most promising material for nonlinear optical devices [1]. The importance of the ternary pnictides $A^{II}B^{IV}C_2^V$ became even more eminent with the discovery of room-temperature ferromagnetism (RT FM) in highly Mn-doped semiconducting $CdGeP_2$, $ZnGeP_2$ [2] and other pnictides (see references within [3]). At variance with other semiconductors, they open also the possibility to combine the observed RT FM with their excellent nonlinear optical properties, resulting in a new class of material for nonlinear optics and spintronic applications. The origin of RT FM in Mn-doped II–IV–V_2 remains controversial in literature [2,4–6]. The existence of RT FM is also predicted for other transition metals (TMs) [4]. For Mn-doped II–IV–V_2 compounds, the site preference and valence state for the different TMs and their interaction with native defects play an important role in the discussion [5,7]. The EPR studies of TMs as well as of intrinsic defects in the II–IV–V_2 compounds have been recently reviewed [7]. In addition, Cu_{Zn}^{2+} was found in $ZnGeP_2$ [8], and Cr^{2+} and Cr^{4+} in $CdGeAs_2$ [9]. Latest EPR studies of Mn-doped $ZnGeP_2$ have shown the site inequivalence of Mn^{2+} substituted on Zn site in $ZnGeP_2$ [3].

In this paper we present the first EPR results for Fe- and Cr-related defects in $ZnGeP_2$ and provide direct evidence for the formations of Mn_{Zn}^{2+}–Mn_{Zn}^{2+} pairs in Mn-doped $ZnGeP_2$.

2. Experimental results and analysis

The $ZnGeP_2$ bulk crystals used in this work have been grown by the HGF technique. EPR spectra that originated from native defects [7] are the most common features of

*Corresponding author. Tel.: +49 30 314 26601; fax: +49 30 314 22569.
E-mail address: gehlhoff@sol.physik.tu-berlin.de (W. Gehlhoff).
[1]On leave from the Ioffe Physico-Technical Institute, RAS, 194021 St. Petersburg, Russia.

0921-4526/$ - see front matter © 2006 Elsevier B.V. All rights reserved.
doi:10.1016/j.physb.2005.12.198

these samples. However, the set studied here incorporated a small concentration of Fe and Cr during the grow process. The Mn-doped samples were obtained by varying the Mn concentration in the melt between 0.2 and 5 mol%.

Fig. 1 shows the over-all EPR spectrum obtained in the Q-band (34 GHz) for a low Fe- and Cr-doped $ZnGeP_2$ sample at $T = 40$ K with the magnetic field B parallel to the c-axis. Without illumination we observed in addition to the strong spectrum of the zinc vacancy (V^-_{Zn}) at 1214 mT, one Cr spectrum and two Fe spectra. The Cr spectrum correspond to the valence state Cr^{4+}, and the Fe spectra to Fe^{3+} and Fe^{2+}. Under photoexcitation, additional EPR spectra for Fe^+ and the anti-site defect Ge^+_{Zn} are observed. Below 20 K, the phosphorus vacancy EPR spectrum is also revealed.

The observed tetragonal Fe and Cr defects have orbital singlets as ground state with an electron spin $S \leqslant \frac{5}{2}$. Their EPR spectra can be approximately described with the spin Hamiltonian (SH)

$$\begin{aligned}\mathbf{H} = {} & \mu_B \mathbf{SgB} + D\left[S_z^2 - \frac{1}{3}S(S+1)\right] \\ & + \frac{1}{180}F[35S_z^4 - 30S(S+1)S_z^2 + 25S_z^2 \\ & - 6S(S+1) + 3S^2(S+1)^2] \\ & + \frac{a}{6}\left[S_\xi^4 + S_\eta^4 + S_\zeta^4 - \frac{1}{5}S(S+1)(3S^2+S-1)\right], \qquad (1)\end{aligned}$$

where z is along the c-axis, whereas ξ, η, and ζ ($\equiv z$) refer to the cubic axes at each of the two magnetically nonequivalent Zn(Ge) lattice sites for S_4 symmetry resulting from the clockwise and counterclockwise rotation of the anion tetrahedra around the c-axis by the angle τ [3,10]. For $S<2$, the last two terms in the SH (1) give no contributions and therefore these two sites cannot be distinguished for such spin manifolds. For a complete and exact description of the spectra, some additional terms in the SH (1) resulting from the transformation of the fourth-rank spin operators must be taken into account [3]. This will be done elsewhere in connection with an exact eigenfunctions and eigenvalues calculation including a complete analysis of the X- and Q-band EPR spectra obtained for different crystallographic planes. Here, we will focus only on their main properties. The observed two iron spectra $Fe^{3+}(S=\frac{5}{2})$ and $Fe^+(S=\frac{3}{2})$ show the typical behavior of uneven spin systems with a zero-field splitting (ZFS) largely compared to the Zeeman energy. In the limiting case of ZFS much larger than the Zeeman energy, only spin transitions $-M \rightleftharpoons +M$ can be observed, which can be approximately described by an effective SH $\mathbf{H} = \mu_B \mathbf{Bg'S'}$ with $S' = 1/2$. The dependence of the apparent g'-values of transitions within the $|\pm 1/2\rangle$ spin doublet on the angle θ between the tetragonal axis and the magnetic field B is given for $S = 5/2(3/2;1/2)$ in the first order by $g'(\theta) = \sqrt{g_\parallel^2 \cos^2\theta + k^2 g_\perp^2 \sin^2\theta}$, where $k^2 = 9(4;1)$. The corrections up to the third order in the Zeeman energy for $S = 5/2(3/2)$ are given in Ref. [11]. With $B \| c$ ($\theta = 0^\circ$), the apparent value g' is equal $g_\parallel$, while for $B \perp c$ ($\theta = 90^\circ$) one obtains

$$g'_\perp = 3g_\perp[1 - 1/2(g_\perp \mu_B B/D)^2] \quad \text{for } S = 5/2$$

and

$$g'_\perp = 2g_\perp[1 - 3/16(g_\perp \mu_B B/D)^2] \quad \text{for } S = 3/2. \qquad (2)$$

The Fe^{3+} ($S=\frac{5}{2}$) spectrum shown in Fig. 1 for $B \| c$ consists of three lines at $B = 36$, 1214 mT (masking in this direction by the strong V^-_{Zn} EPR spectrum) and 1640 mT correspond to the allowed $\Delta M = \pm 1$ transitions within the $S = \frac{5}{2}$ manifold. The measured angular dependence of the Fe^{3+} line positions in the X-band is presented in Fig. 2. Since the intensity of the transitions strongly depends on the rotation angle, some of the lines are not observed for all magnetic field directions. The low-field resonance line between 140 and 330 mT indicates tetragonal symmetry of the spectrum and can be well described within the effective $S' = \frac{1}{2}$ approach with the g-values, $g'_\parallel = 2.0$ and $g'_\perp = 5.96$. The small deviation from $g'_\perp = 6$ and the detection of several other groups of lines in Fig. 2 indicates that the fine structure splitting is not much different from the Zeeman splitting. The line at 540 mT for $B \| [0\,1\,0]$ arises from the transition $-3/2 \rightleftharpoons +3/2$ (high-field designation). This transition is forbidden in the parallel orientation ($\theta = 0^\circ$) but allowed in the perpendicular one ($\theta = 90^\circ$) as the states are heavily mixed. From the observed looping transition $\pm 1/2 \leftrightharpoons \pm 3/2$ between 900 and 1200 mT, one obtains $|2D - 5/2(a + 2/3F)| = 1.37\,\text{cm}^{-1}$. With $g_\perp \approx g_\parallel$ and $2D = 1.3\,\text{cm}^{-1}$, we obtain $g'_\perp = 5.97$, which is in good agreement with the experimental result. The looping lines around $\theta = 0$ between 450 and 770 mT are caused by $+1/2 \leftrightharpoons -3/2$ transitions. Rotating the magnetic field in

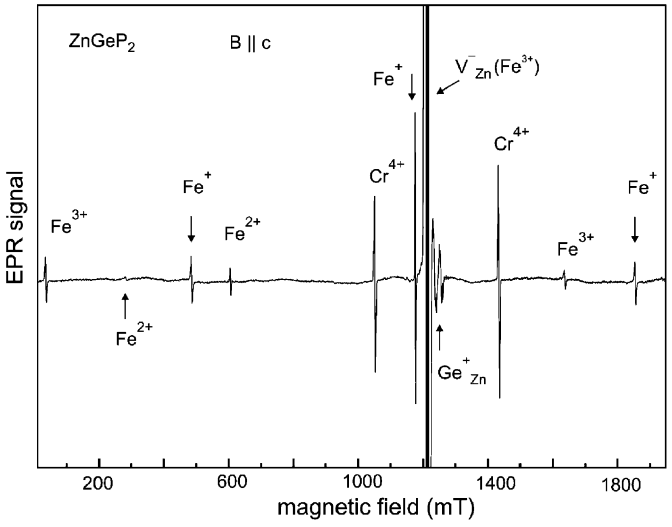

Fig. 1. Overall EPR spectrum of Fe- and Cr-contaminated $ZnGeP_2$ recorded for $B \| c$ at 34 GHz and $T = 40$ K. The Fe^{3+} transition at $B = 1214$ mT is covered by the strong EPR signal produced by the zinc vacancy (V^-_{Zn}). The transitions assigned to Fe^+ and anti-site defect Ge^+_{Zn} are only observed under illumination of the sample.

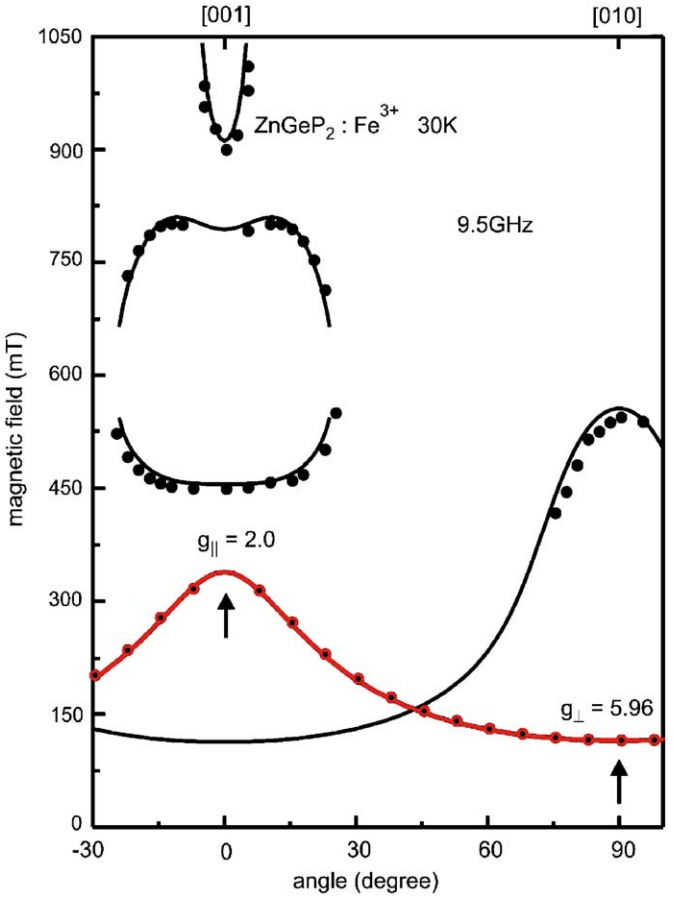

Fig. 2. Angular dependence of the experimental line positions (●) of $ZnGeP_2$:Fe^{3+} obtained at 9.48 GHz and $T = 30$ K. The magnetic field is rotated in the (1 1 0) plane. The solid lines are calculated from the generalized SH (1) given in Ref. [3] with fitted parameters. The bold low-field line corresponds to transition within the Kramers doublet $|\pm 1/2\rangle$, which can be described with the effective g-values $g'_{\parallel} = 2.0$ and $g'_{\perp} = 5.96$ (see text).

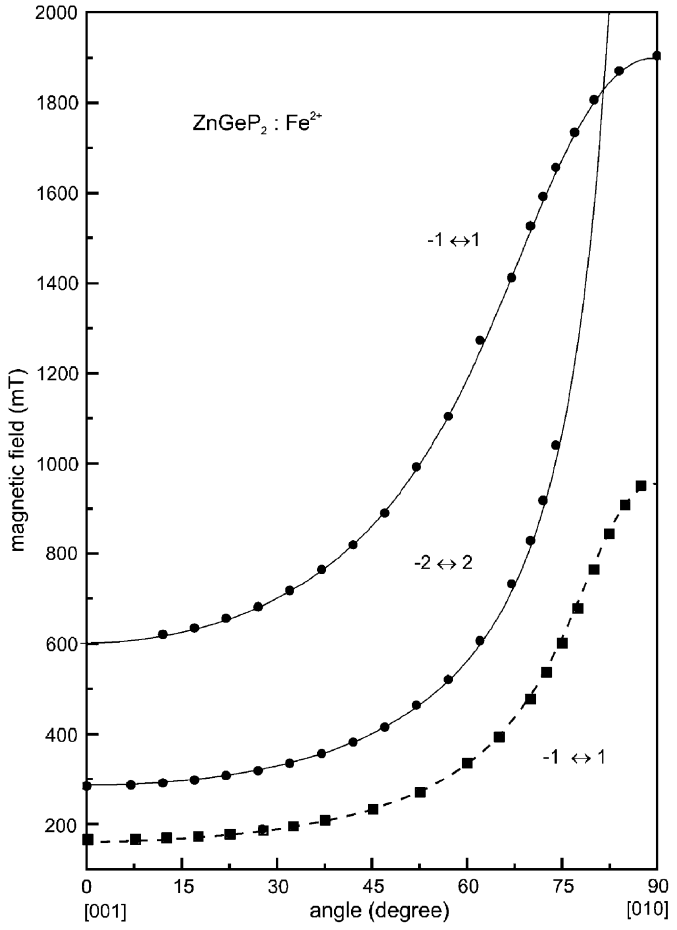

Fig. 3. Angular dependence of the observed X-band (■) and Q-band (●) Fe^{2+} EPR transitions in $ZnGeP_2$. The magnetic field is rotated in the (1 0 0) plane. In the X-band (9.48 GHz) only the $-1 \rightleftharpoons +1$ transitions can be detected (see text). The solid and dashed lines are a computer fit to the experimental data.

the (1 0 0) plane, we observed both an uncommon strong variation of the line position caused by the large value of the fourth-order spin parameter a ($a \approx 0.03\,\mathrm{cm}^{-1}$) and a splitting of the fine-structure lines revealing the site inequivalence of the cation site. From this splitting, we determined the Fe^{3+}-induced tilting angle as $\tau_{Fe} = 7.6^{\circ}$, which is roughly two degree larger than the value for Mn^{2+} at Zn lattice site in $ZnSiP_2$ and $ZnGeP_2$ [3].

The spectrum of the non-Kramers ion Fe^{2+} (d^6, ^5D) with $S = 2$ shown in Fig. 1 consists of two lines at $B = 284$ and 606 mT that correspond to the transitions $-2 \leftrightharpoons +2$ and $-1 \leftrightharpoons +1$ within a $^5\hat{A}$ ($^5T_1$) ground state. The large D value leads within the $S = 2$ manifold to a splitting into the spin states $M = 0, \pm 1, \pm 2$, the last two being split by the cubic-field parameter a [see Eq. (3)]. The complete angular dependence of the Fe^{2+} spectrum is shown in Fig. 3. The intensity is very week for $B||c$ and increases as B approaches the perpendicular direction. In the X-band, only the transition $-1 \leftrightharpoons +1$ can be observed indicating that the splitting of the non-Kramers doublet $|\pm 2\rangle$, caused by the fourth-order spin terms in Eq. (1), is larger than the microwave energy. The line position of this transition varies with the angle θ between the magnetic field direction and c-axis approximately, according to

$$B = \frac{1}{g_{\parallel}^{\mathrm{eff}} \mu_B \cos\theta} \sqrt{(h\nu)^2 - a^2}, \tag{3}$$

where $g_{\parallel}^{\mathrm{eff}} = 4g_{\parallel}$. If B is rotated in the (0 0 1)-plane, the $-1 \leftrightharpoons +1$ exhibits a marked cubic anisotropy from which we estimate $a \approx -1\,\mathrm{cm}^{-1}$. The temperature dependence of the $-2 \leftrightharpoons +2$ transition gives evidence that $D > 0$, that means, ground state is the spin state $M = 0$.

The Cr-related spectrum observed without photo-excitation is assigned to Cr^{4+} ($3d^2$) on Ge site. Its angular variation is shown in Fig. 4. The complete analysis of this spectrum obtained in the X- and Q-band provides evidence that it can only be generated by transitions within an orbital singlet ground state $^3A_2$ with $S = 1$ from a $3d^2$ (^3F) configuration. The fine structure transitions can be described with $g_{\parallel} = 1.986$, $g_{\perp} = 1.984$ and

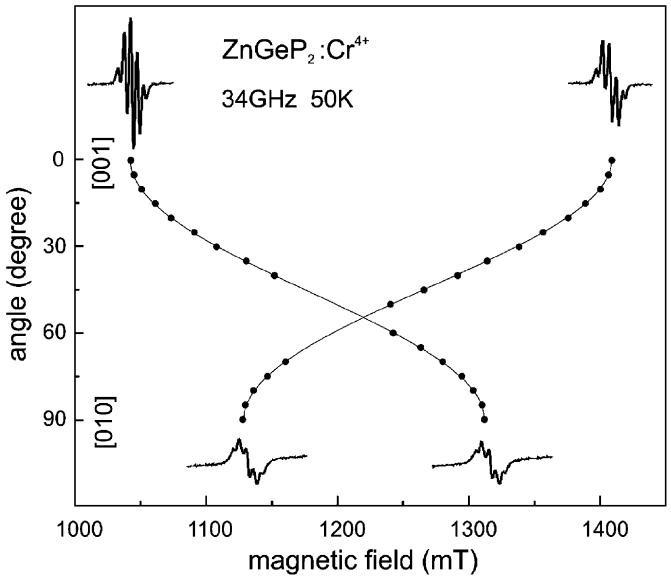

Fig. 4. Angular dependence of Cr^{4+}_{Ge} in $ZnGeP_2$ in the Q-band. The two transitions $0 \rightleftharpoons \pm 1$ exhibit a well-resolved characteristic five line multiplets with the intensity ratios 1:4:6:4:1 due to the interaction with four equivalent ^{31}P ($I = 1/2$, 100% natural abundance).

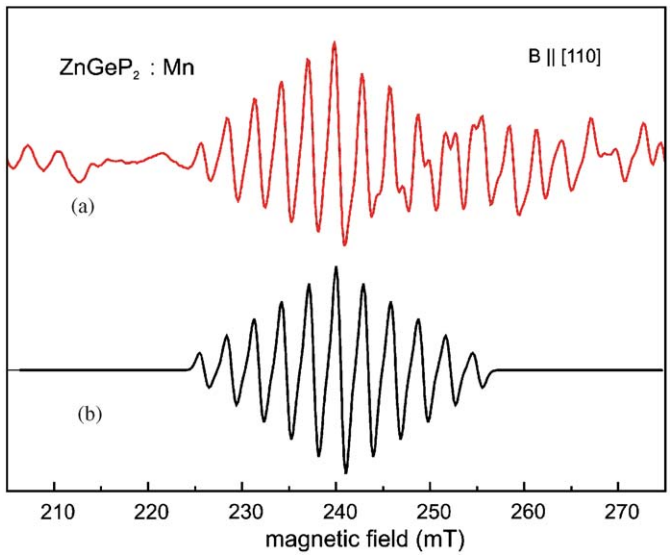

Fig. 5. Resolved HF interaction of Mn^{2+}_{Zn}–Mn^{2+}_{Zn} pairs in $ZnGeP_2$ for $B \| [1\,1\,0]$ at 5 K for the transitions $-1 \rightleftharpoons +0$ of the spin state $S = 1$, which is partly overlapped on the high-field side with a transition within the spin state $S = 2$ (a). For the simulated structure (b), the half HF splitting of the isolated Mn^{2+}_{Zn} of $|A| = 52.8 \times 10^{-4}\,cm^{-1}$ [3] and the characteristic intensity ratio of the 11 HF lines of such pair were used.

$D = 0.1696\,cm^{-1}$. The two transition $0 \leftrightharpoons \pm 1$ exhibit a well-resolved characteristic five line multiplets with the intensity ratios, 1:4:6:4:1 due to the interaction with four equivalent ^{31}P nuclei.

Illuminating the iron containing samples, with light below the band gap at $T \leqslant 60\,K$, we observed a new EPR spectrum showing the characteristic behavior of an orbital singlet with spin $S = \frac{3}{2}$ in a strong tetragonal distorted cubic crystal field that can be described with the effective spin $S' = \frac{1}{2}$ and the apparent g'-values $g'_{\|} = 2.902$ and $g'_{\perp} = 4.021$. This photo-generated spectrum arose from Fe^{+} ($3d^7$, ^4F) with a $^4A_2$ ground state. We observed in n-type $ZnSiP_2$:Fe, a corresponding Fe^{+} spectrum with $g'_{\|} = 2.114$ and $g'_{\perp} = 4.271$ without photo-excitation [12].

For nearly perfect Mn-doped $ZnGeP_2$ crystals we observed anti-ferromagnetically coupled Mn^{2+}_{Zn}–Mn^{2+}_{Zn} pairs. This is evidenced by the temperature dependence of the different transition within the spin multiples having total spins $S = 0, 1, 2, 3, 4, 5$ and their characteristic hyperfine structure produced by the interaction of the two ^{55}Mn nuclei with $I = 5/2 : 11$ hyperfine lines with the intensity ratio 1:2:3:4:5:6:5:4:3:2:1, as well as the half hyperfine splitting observed for isolated Mn^{2+} on Zn site (Fig. 5). A complete analysis of this study will be given elsewhere.

3. Conclusion

Low doping of $ZnGeP_2$ during the HGF growth process, simultaneously with Fe and Cr in low concentrations result both in the substitution of Ge^{4+} on lattice site by $Fe^{3+}(B^-)$, and $Cr^{4+}(B^0)$ as well as of Zn^{2+} lattice site by $Fe^{2+}(A^0)$. The site preference of the TM in the different charge states is important since substitution on lower valent states generate donors, whereas substitution on a higher valent states generate acceptors. Therefore, there is only the substitution of the negatively charged acceptor Fe^{3+} on the higher valent states Ge^{4+} due to a releasing of charge carriers (holes) and only this substitution can contribute to the generation of a charge-mediated ferromagnetism. According to Dietl's work, only holes are expected to lead to ferromagnetism [13]. The detected photo-induced recharging of Fe^{2+}_{Zn} to Fe^{+}_{Zn} exhibits that the negatively charged acceptor state $Fe^{+}(A^-)$ is similar as in $ZnSiP_2$ within the bandgap. No strong shift of the Fermi level is expected in the low-doped crystals because it is determined in HGF-grown crystals by high concentration of mutually compensating native defects [7]. The detected similar high concentration of native defects and their identical photo-EPR behavior, compared to undoped samples indicate that the Fermi level is hardly modified. Consolidated findings on the role of TMs by the generation of ferromagnetism in II–IV–V_2 compounds can be expected by detailed studies of their site preference as a function of their concentration and the position of the Fermi level as well as the study of the pair and small cluster formation for higher doping concentrations.

References

[1] M.C. Ohmer, R. Pandey, Mater. Res. Bull. 23 (7) (1998) 16.
[2] K. Sato, G.A. Medvedkin, T. Ishibashi, S. Mitani, K. Takanashi, Y. Ishida, D.D. Sarma, J. Okabayashi, A. Fujimoro, T. Kamatani, H. Akai, J. Phys. Chem. Sol. 64 (2003) 1461.

[3] W. Gehlhoff, D. Azamat, V.G. Voevodin, A. Hoffmann, Phys. Status Solidi B 242 (2005) R14.
[4] T. Kamantani, H. Akai, Phase Transitions 76 (2003) 401.
[5] P. Mahadevan, A. Zunger, Phys. Rev. Lett. 88 (2002) 47205.
[6] T. Kwang, J.H. Shim, S. Lee, Appl. Phys. Lett. 83 (2003) 1809.
[7] W. Gehlhoff, D. Azamat, A. Hoffmann, Mater. Sci. Semicond. Process 6 (2003) 379.
[8] K.T. Stevens, L.E. Halliburton, S.D. Setzler, P.G. Schunemann, T.M. Pollak, J. Phys.: Condens. Mater. 15 (2003) 1625.
[9] N.Y. Garces, N.C. Giles, L.E. Halliburton, K. Nagashio, R.S. Feigelson, P.G. Schunemann, J. Appl. Phys. 94 (2003) 7567.
[10] U. Kaufmann, A. Räuber, J. Schneider, Phys. Status Solidi B 74 (1976) 169.
[11] J. Kreissl, W. Gehlhoff, P. Omling, P. Emanuelson, Phys. Rev. B 42 (1990) 1731.
[12] W. Gehlhoff, D. Azamat, A. Krtschil, A. Hoffmann, A. Krost, Physica B 340–342 (2003) 933.
[13] T. Dietl, Science 287 (2000) 1019.